Available online at www.sciencedirect.com
SCIENCE DIRECT®
Journal of Solid State Chemistry 174 (2003) 431–440
JOURNAL OF SOLID STATE CHEMISTRY
http://elsevier.com/locate/jssc

Effect of doping and temperature on the crystal structure of $(V_{1-x}Mo_x)_2O_3$ above and below the metal/insulator transition

C. Tenailleau,[a] E. Suard,[b] J. Rodriguez-Carvajal,[c] A. Gibaud,[d] and P. Lacorre[a,*]

[a] *Laboratoire des Fluorures, UMR CNRS 6010, Université du Maine, Avenue Olivier-Messiaen, F-72085 Le Mans Cedex 9, France*
[b] *Institut Laue Langevin, Avenue des Martyrs, B.P. 156, F-38042 Grenoble Cedex 9, France*
[c] *Laboratoire Léon Brillouin (CEA-CNRS), Centre d'Etudes de Saclay, F-91191 Gif-sur-Yvette Cedex, France*
[d] *Laboratoire de Physique de l'Etat Condensé, UMR CNRS 6087, Université du Maine, F-72085 Le Mans Cedex 9, France*

Received 12 February 2003; received in revised form 14 May 2003; accepted 17 May 2003

Abstract

The crystal structure of new molybdenum-doped vanadium sesquioxides $(V_{1-x}Mo_x)_2O_3$ ($0 \leqslant x \leqslant 0.20$) has been studied at low temperature (10 K) and up to room temperature, through neutron and X-ray powder diffraction. The transition from insulating I- to metallic M-type phases, either by doping or thermally driven, is accompanied by an abrupt decrease of all interatomic distances. Within each structural type however, at 10 K, the effect of doping is essentially the same as at room temperature: it increases cation–oxygen distances, and decreases cation–cation distances, making the cationic coordination octahedra more regular. Thermal effects differ for each phase type: all interatomic distances normally increase in the M-type phase (but with different octahedral modifications depending on doping), but they decrease or remain constant in the I-type phase. This produces an unusual negative thermal expansion coefficient up to 5% at low temperature for the doped compounds.

Keywords: Mo-doped vanadium sesquioxide V_2O_3, Mo^{3+}, V^{3+} oxide; Low-temperature X-ray and neutron powder diffraction; Rietveld structural refinement; Phase transformation; Metal–insulator transition; Interatomic distances; Negative thermal expansion coefficient

1. Introduction

Vanadium sesquioxide is well known and is studied for its abrupt metal/insulator (MI) transition [1,2] around 160 K, considered as a typical example of Mott transition [3], and its various possibilities of doping (see, for instance, Refs. [4,5], and references therein). Recently, we discovered [6] a new family of doped vanadium sesquioxide $(V_{1-x}Mo_x)_{2-\delta}O_3$ ($\delta \leqslant 0.0002$), Mo^{3+} being the first trivalent element of the 4d series, as possible substituent for vanadium in V_2O_3 [7]. The effect of Mo doping on the room temperature corundum-type crystal structure of vanadium sesquioxide has been detailed in a previous paper [8]. Our earlier studies showed that substitution by molybdenum induces, in contrast to any other doping, an increase of the c/a hexagonal cell parameter ratio (c increases while a decreases). Simultaneously, the cation–oxygen distances are longer (in agreement with a trivalent oxidation state of molybdenum) and the cationic octahedral coordination sphere is more regular. Counterintuitively, given the larger size of Mo^{3+}, the intercationic distances decrease upon substitution, which was postulated to result from the establishment of Mo–Mo metal bonding [8].

In the current paper, we present a low-temperature study (between 10 K and 300 K) of the influence of Mo doping on this structure. Above the MI transition, V_2O_3 adopts a rhombohedral symmetry (space group $R\text{-}3c$); at low temperatures the symmetry is lowered to monoclinic phase (space group $I2/a$, usually used instead of standard $C2/c$) due to a severe lattice distortion, with loss of the three-fold rotoreflection axes. Partial substitution of trivalent vanadium by trivalent molybdenum induces a lowering of the MI transition temperature similar to the substitution by trivalent titanium, with stabilization of the metallic phase in the whole temperature range for doping rates higher than 6% [6]. The monoclinic phase of $(V_{1-x}Mo_x)_{2-\delta}O_3$, therefore, only exists at the lowest temperatures in the

*Corresponding author. Fax: +33-2-4383-3506.
E-mail address: philippe.lacorre@univ-lemans.fr (P. Lacorre).

0022-4596/03/$ - see front matter © 2003 Elsevier Inc. All rights reserved.
doi:10.1016/S0022-4596(03)00295-0

range $0 \leqslant x < 0.06$. In the current study, we used low-temperature neutron and X-ray powder diffraction to examine the structural distortions induced by both cooling and Mo doping on V_2O_3. Note that such systematic low-temperature structural studies on vanadium sesquioxide systems are rather rare, probably because the MI transition is destructive of single crystals, and because vanadium has a negligible cross-section for neutrons. Section 2 is devoted to the experimental procedures. In Section 3, we present the effect of Mo doping on the crystal structure of the I-type and M-type phases at 10 K, and compare it to the same effect on the M rhombohedral phase presented in the previous paper [7]. The thermal evolution of both structures between 10 and 300 K will be presented and analyzed in Section 4. Finally a comparison and conclusion will be drawn in Section 5.

2. Experimental

2.1. Synthesis

The powder samples were prepared from stoichiometric mixtures of V_2O_3 and MoO_2 heated in a high-frequency induction furnace under vacuum (about 10^{-6} mbar) at 870°C (see Ref. [6] for details). This process was repeated several times, with intermediate grindings, in order to obtain several grams of pure materials necessary for the crystallographic study. In order to prevent oxidation (Tenailleau et al., submitted), the samples were kept in a glove box under less than 10 ppm of oxygen.

2.2. Structural characterization

The structural characterization was carried out using low-temperature powder X-ray and neutron diffraction. X-ray diffraction patterns were recorded on a two-circle diffractometer equipped with a Huber 424 goniometer, a PW 1130/00/60 Philips generator and an LTS-21 Displex cryogenerator (temperature range [10–300 K], 2θ domain 20–126.2°, 2θ step 0.03°, time/step 15 s). Neutron diffraction patterns were collected on Debye–Scherrer diffractometers D2B (ILL Grenoble, $\lambda = 1.5941$ Å, 2θ domain 10–158°, 2θ step 0.05°, 5 scans 85 000 or 95 000cts) for $x = 0\%$, 3%, 5%, 10%, and 3T2 (LLB Saclay, $\lambda = 1.2252$ Å, 2θ domain 10–125.45°, step 0.05°, scan 50 000 or 80 000cts) for $x = 2\%$, 20%. The Rietveld program FullProf [9] was used for structural refinement. The structural refinements at 10 K were performed simultaneously on the neutron and X-ray diffraction patterns with a 50–50% weighting scheme. Fig. 1 presents the refined patterns for $x = 5\%$, with contribution of both I-type and M-type phases (see below). The neutron diffraction fits of the I-type phases take into account the magnetic diffraction peaks, which will be analyzed in a subsequent paper devoted to the magnetic behavior of this system (Tenailleau et al., in preparation).

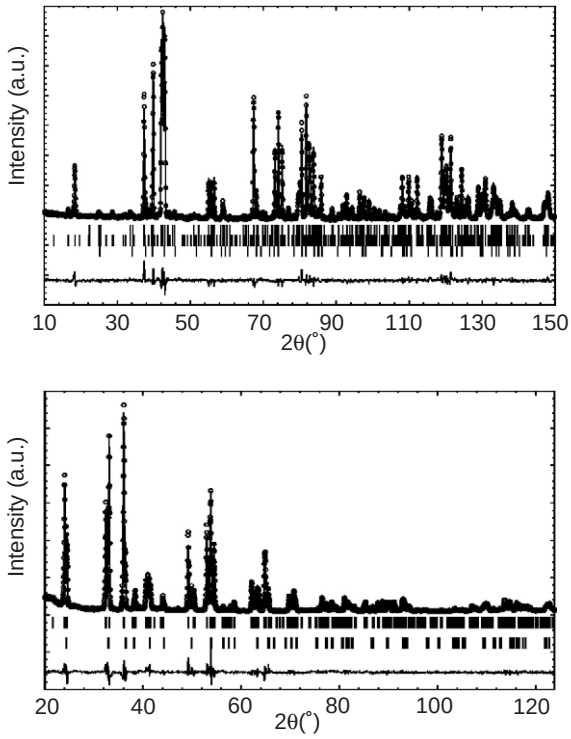

Fig. 1. 10 K X-ray (top) and neutron (bottom) diffraction patterns of $(V_{0.95}Mo_{0.05})_2O_3$ and coupled 50–50% X-ray/neutron Rietveld refinements. Reliability factors (R_B and R_F for I-type/M-type phases): for X-rays, $R_p = 0.129$, $R_{wp} = 0.147$, $R_{exp} = 0.061$, $\chi^2 = 5.83$, $R_B = 0.069/0.053$, $R_F = 0.058/0052$; for neutrons $R_p = 0.115$, $R_{wp} = 0.106$, $R_{exp} = 0.061$, $\chi^2 = 2.97$, $R_B = 0.048/0.055$, $R_F = 0.032/0.0.045$. Observed = dots, calculated = lines, difference below. Vertical bars mark the reflexion positions, from top to bottom: I-type phase, magnetic contribution (neutron only), M-type phase.

3. Crystal structures at 10 K as a function of doping

Fig. 2 displays a series of low-temperature X-ray diffraction patterns of $(V_{1-x}Mo_x)_2O_3$ ($x = 3\%$) showing the transition from rhombohedral M-type phase (high T) to monoclinic I-type phase (low T). The thermal evolution of the relative amount of rhombohedral phase for different Mo-doping rates is presented in Fig. 3, and shows evidence of hysteresis at the transition. The large size of this hysteresis, especially for 5% Mo, is consistent with the strong first-order character of the transition, with low phase nucleation rate at low temperature. At 10 K, the I-type phase is observed up to an Mo doping of 5%. This last composition is biphasic at 10 K, with about 20% of rhombohedral phase, whereas the 10%

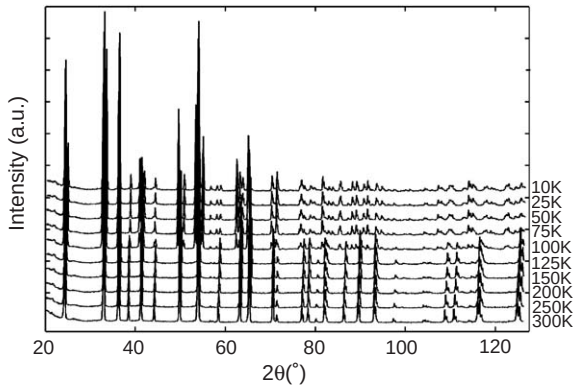

Fig. 2. Cooling low-temperature X-ray thermodiffractograms of $(V_{0.97}Mo_{0.03})_2O_3$.

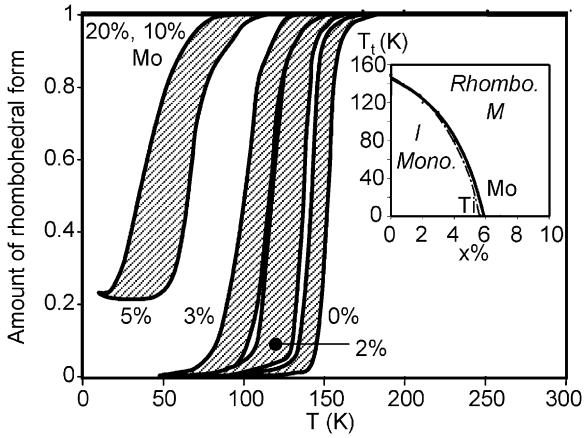

Fig. 3. Amount of rhombohedral M-type phase as a function of temperature in $(V_{1-x}Mo_x)_2O_3$. Hatched regions correspond to hysteresis cycles at the first-order transition. Inset: the corresponding temperature/composition phase diagram, and comparison with the Ti-doped system [12].

and 20% substituted sesquioxides retain the rhombohedral symmetry down to the lowest temperature.

3.1. Cell parameters

Fig. 4 displays the reduced cell volume evolution upon Mo doping at 10 K, compared to those of the M-type phase at 150 K and 300 K. All three cell volumes increase in a roughly parallel manner, due to the larger size of Mo^{3+} relative to V^{3+}. The abrupt volume drop observed at 5% Mo between the two phases is due to electron delocalization in the low-temperature M-type phase, as observed at insulator/metal type transitions.

Table 1 contains the cell parameter variation with doping in the I- and M-type phases at 10 K. Direct comparison between the two systems can be made through the transformation matrix between the rhombohedral and monoclinic crystal cells [10]:

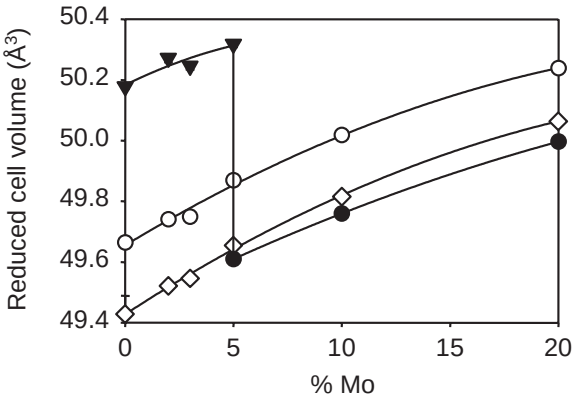

Fig. 4. Reduced cell volume evolution with the doping rate in $(V_{1-x}Mo_x)_2O_3$ at different temperatures: Open circles = 300 K (M-type phase), diamonds = 150 K (M-type phase), triangles = 10 K (I-type phase) and black circles = 10 K (M-type phase).

$$\begin{bmatrix} a_m \\ b_m \\ c_m \end{bmatrix} = \begin{bmatrix} 2/3 & 4/3 & 1/3 \\ 1 & 0 & 0 \\ 1/3 & 2/3 & -1/3 \end{bmatrix} \begin{bmatrix} a_h \\ b_h \\ c_h \end{bmatrix}.$$

From this matrix, the M rhombohedral phase can be described in equivalent monoclinic parameters, which allows us to compare the influence of Mo doping on the I- and M-type phases at 10 K and on the M-type phase at room temperature (see Fig. 5). Aside from the large difference between the M- and I-type parameters (due to the abrupt first-order transition), all the curves evolve roughly in parallel, an indication that Mo doping has quantitatively the same influence on the cell of the M- and I-type phases. Fig. 6 gives a more synthetic, less rigorous but perhaps more suggestive comparison between the two phases within the pseudo-hexagonal description.

3.2. Structural modification

Fig. 7 shows representative projections of the monoclinic structure. In the more symmetric rhombohedral form two projections, along the hexagonal c_h-axis (π_h plane) and perpendicular to it (π plane), are necessary in order to depict all nearest-neighbor distances and angles of the structure (see Ref. [7]). In the low-temperature monoclinic form, the loss of the three-fold axis induces a loss of the structural equivalence between the three π planes originally linked by the rotoreflection axis, into one plane (π_1) perpendicular to b_m, and two planes (π_2 and π'_2) symmetrical through the remaining two-fold axis. In Fig. 7, these planes are projected along specific directions of the monoclinic cell:

- π_h plane ($(10\text{-}1)_m$ plane, equivalent to the hexagonal plane of M phase) is viewed along direction $[10\text{-}2]_m$,

Table 1
Refined cell parameters of the monoclinic and rhombohedral (hexagonal setting) phases at 10 K for the studied Mo-doping rates

x% Mo (sym)	a (Å)	b (Å)	c (Å)	β (°) or c/a^*	V (Å^3)
0% (mono)	7.2741(2)	5.0053(1)	5.5514(2)	96.779(1)	200.71(1)
2% (mono)	7.2855(3)	5.0012(2)	5.5592(2)	96.886(2)	201.10(2)
3% (mono)	7.2868(3)	4.9974(2)	5.5590(2)	96.926(1)	200.96(2)
5% (mono)	7.3039(2)	4.9875(1)	5.5646(2)	97.141(1)	201.14(1)
5% (hex)	4.9323(2)		14.1207(6)	2.863*	297.50(2)
10% (hex)	4.9290(2)		14.1888(5)	2.879*	298.53(2)
20% (hex)	4.9209(2)		14.3050(5)	2.907*	299.99(2)

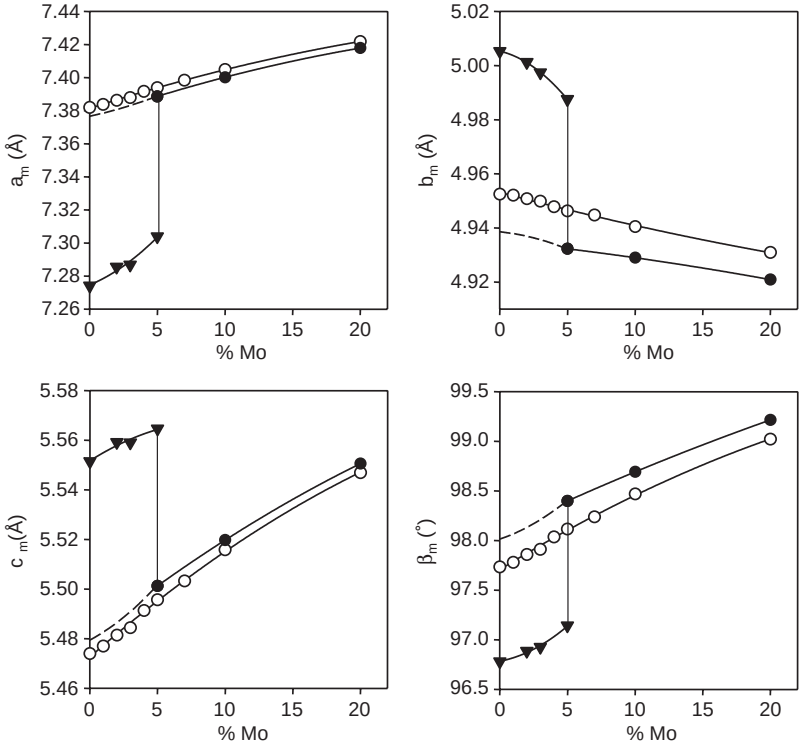

Fig. 5. Evolution with Mo doping of the 10 K cell parameters in a monoclinic description (black symbols). The abrupt jumps correspond to a change from monoclinic (low doping rate) to rhombohedral (high doping rate) symmetry. For comparison, the room temperature cell parameters evolution is given (open circles). For the transcription of rhombohedral to monoclinic parameters (circles) see text. Dashed line = extrapolation of high-doping-rate parameters.

- π_1 plane $(010)_m$ is projected along $[010]_m$,
- π_2 plane viewed along $[111]_m$, is structurally equivalent to π'_2 plane along $[-11-1]_m$.

All interatomic distances and angles of the monoclinic phase can be found in the three planes π_h, π_1 and π_2.

Structurally speaking, in the low-temperature phase, the oxide ions are split into two independent crystallographic positions, whereas cations, which were located on the three-fold axis in the high-temperature phase, are now in the most general position of the monoclinic space group. It means that the cationic pairs belonging to edge-sharing bioctahedral units are no longer perpendicular to the π_h plane, so also the stacking of these planes. Both deviations can be used as a quantitative measures of the monoclinic distortion. It can be seen in Fig. 8 that they both decrease upon Mo doping and collapse above 5% Mo, with stabilization of the hexagonal form.

Table 2 provides the atomic parameters of all studied substituted compounds at 10 K.

From these results, it appears interesting to follow the evolution of distances between nearest cations and anions as a function of doping, and to compare this to

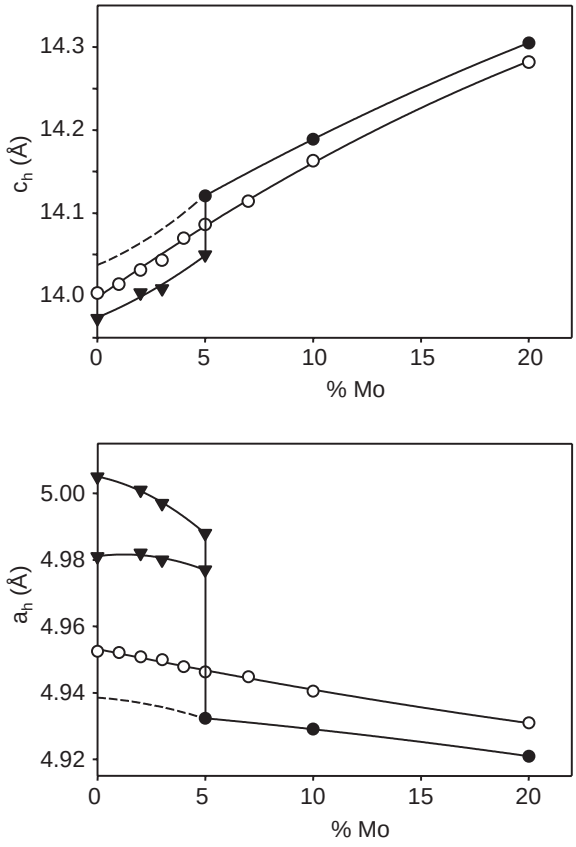

Fig. 6. Same as Fig. 5, but in an hexagonal description. The two sets of a_h parameters at low doping rates (triangles) derive from the lower symmetry of the monoclinic cell (inequivalent π_1 and π_2 planes).

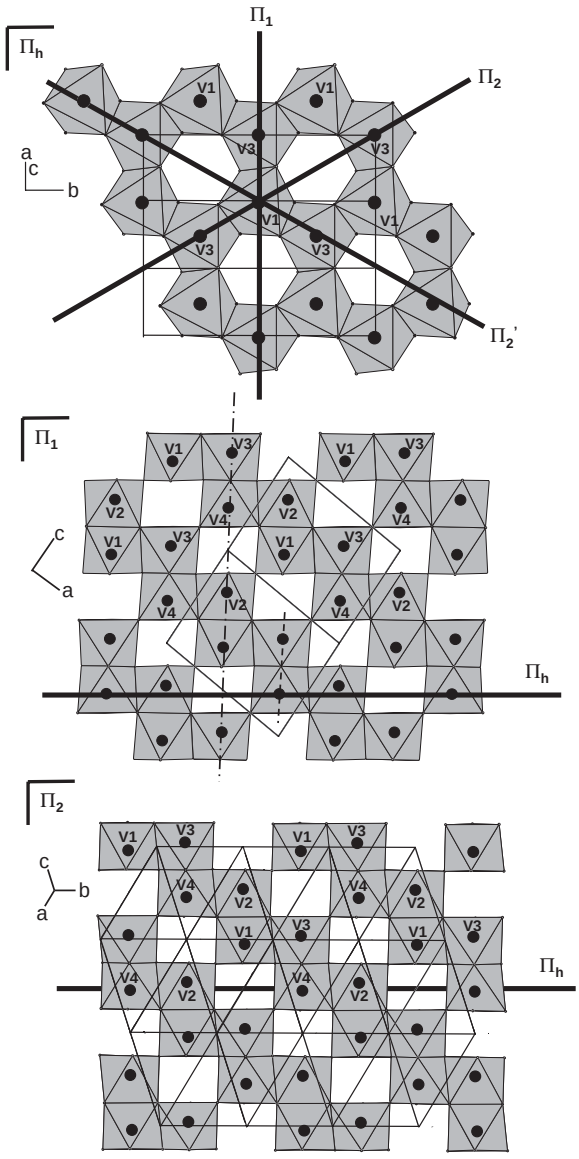

Fig. 7. Projections of the monoclinic structure of V_2O_3, showing the main planes discussed in the text. The dashed and dot-dashed vertical lines indicate the directions of bioctahedral pairs and of layer stacking, respectively (see text and Fig. 8). The cationic numbering corresponds to that adopted in Ref. [8] for the rhombohedral phase.

our previous similar analysis at room temperature [8]. Additional interest derives from the transition between the two phases, which does not occur at room temperature. Fig. 9 displays such curves for average cation–cation and cation–anion distances. First of all, the same abrupt drop, already evidenced at the phase transition for cell volume (see Fig. 4), is observed for all distances whatever their type. Aside from this point, the same general trend upon Mo doping as that observed at room temperature is present at low temperature: cation–cation distances generally decrease while cation–anion distances increase. If this last effect appears to be somewhat natural, given the larger size of trivalent molybdenum, that of cations getting closer is rather counterintuitive. We have previously interpreted this as resulting from the progressive incidence of Mo–Mo clusters in adjacent octahedra, with concomitant establishment of metal–metal bonding [8]. Such an effect is, however, less uniform in the I-type phase, as can be seen in Fig. 10 for larger in-π_h-plane cation–cation distances: while two such distances decrease upon doping, the third increases.

Concerning octahedral distortion, the effect of substitution by molybdenum is globally similar in the I-type phase to that observed in the M-type phase at room temperature [8]. Expansion of faces shared by bioctahedral units and compression of opposed faces tend to make the octahedron more regular, and oxygen stacking closer to compactness. Fig. 11 gives a projection on the three planes, π_h, π_1 and π_2, of the relative atomic displacements (exaggerated).

4. Thermal evolution

We have followed the structural thermal evolution of both I- and M-type phases using low-temperature X-ray

diffraction only. The absence of isothermal neutron diffraction patterns made the structural refinements less accurate, especially for oxide ion positioning, but we nevertheless were able to depict the main tendencies.

4.1. Cell parameters

Fig. 12 (upper row) gives the thermal evolution of the M-type phase cell parameters for different doping rates. Note that the thermal expansion is highly anisotropic, since one of the cell parameters decreases with temperature, while the other increases, whatever the doping level (all the curves evolve in parallel). Also, the c/a ratio increases when temperature decreases, which means that the highest c/a ratio in this series (and probably of all the known sesquioxides) is obtained for 20% Mo doping at low temperature.

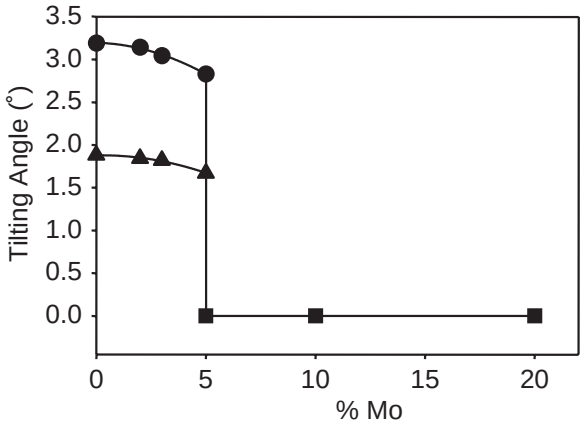

Fig. 8. Effect of molybdenum substitution on the cell distortion at 10 K, measured as the deviation from perpendicularity to the π_h plane of layer stacking (triangles) and bioctahedral units (circles). See text and Fig. 7.

The thermal evolution of the I-type phase cell parameters is displayed in Fig. 12 (lower row). Contrary to what is observed in the M-type phase, they do not evolve the same way for all Mo-doping rates. The most remarkable and unexpected consequence is that, whereas undoped V_2O_3 exhibits a regular thermal expansion, this is no longer the case for Mo-doped compounds, which show a thermal contraction (Fig. 13). Such unusual negative thermal expansion coefficients have already been observed in some other oxides such as molybdate $Sc_2Mo_3O_{12}$ or tungstates $Sc_2W_3O_{12}$ or $Zr_2WP_2O_{12}$, for instance, [11]. In the I-type phase of $(V_{1-x}Mo_x)_{2-\delta}O_3$ thermal contraction is anisotropic, for instance, for $x=0.05$ a and c parameters decrease while b increases with temperature.

Finally when reduced cell volumes are considered for both phases, the transition from I-type to M-type phase is accompanied by an abrupt decrease of cell volume, due to electron delocalization in the most conducting phase. The same type of cell volume reduction was observed at 10 K upon Mo doping (see Fig. 4).

4.2. Crystal structure

An accurate determination of the crystal structure thermal evolution would have required mixed refinements from neutron and X-ray diffraction patterns recorded at each temperature, as was done at 10 K (see above) and room temperature [8]. Since we only have

Table 2
Refined (from coupled neutron and X-ray data) atomic parameters of the monoclinic and rhombohedral (hexagonal setting) phases at 10 K for the studied Mo-doping rates

x% Mo (sym)	Atom	Site	x	y	z	B (Å^2)
0% (mono)	V	8*f*	0.3445(2)	0.0025(8)	0.3001(2)	0.41(3)
	Of	8*f*	0.4043(3)	0.8493(4)	0.6459(4)	0.31(4)
	Oe	4*e*	1/4	0.3166(6)	1/2	0.35(6)
2% (mono)	C(V/Mo)	8*f*	0.3445(2)	0.0031(10)	0.3001(2)	0.56(4)
	Of	8*f*	0.4042(3)	0.8481(4)	0.6459(4)	0.24(4)
	Oe	4*e*	1/4	0.3177(6)	1/2	0.36(6)
3% (mono)	C(V/Mo)	8*f*	0.3442(2)	0.0044(8)	0.3014(2)	0.42(3)
	Of	8*f*	0.4044(3)	0.8495(4)	0.6469(4)	0.31(4)
	Oe	4*e*	1/4	0.3163(6)	1/2	0.27(6)
5% (mono)	C(V/Mo)	8*f*	0.3439(2)	0.0063(7)	0.3026(2)	0.46(4)
	Of	8*f*	0.4050(3)	0.8477(4)	0.6474(4)	0.43(3)
	Oe	4*e*	1/4	0.3180(5)	1/2	0.41(5)
5% (rhomb)	C(V/Mo)	12*c*	0	0	0.3444(3)	0.44(10)
	O	18*e*	0.3143(14)	0	1/4	0.40(11)
10% (rhomb)	C(V/Mo)	12*c*	0	0	0.3444(2)	0.49(4)
	O	18*e*	0.3153(4)	0	1/4	0.42(3)
20% (rhomb)	C(V/Mo)	12*c*	0	0	0.3433(1)	0.44(4)
	O	18*e*	0.3164(4)	0	1/4	0.31(3)

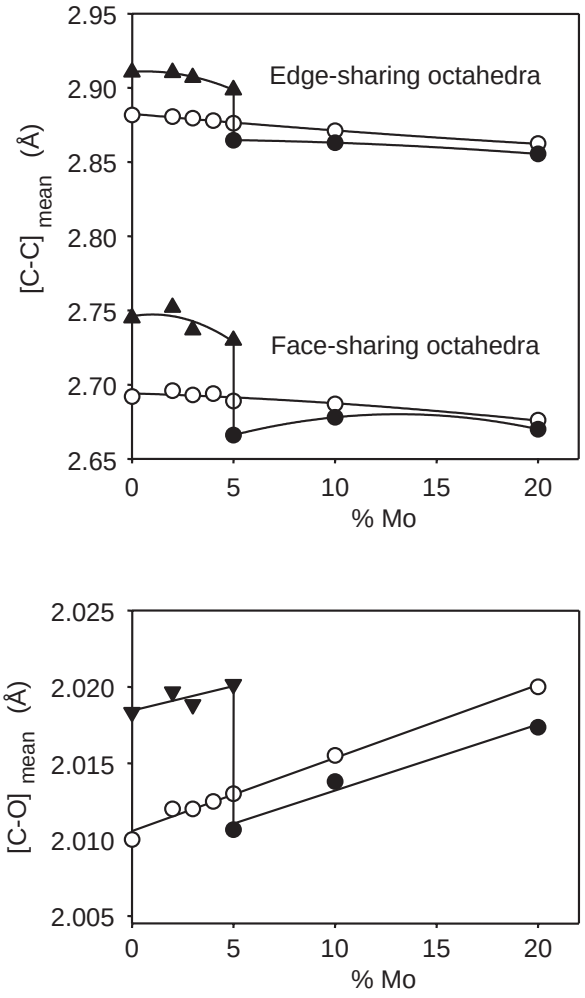

Fig. 9. Average interatomic distances in $(V_{1-x}Mo_x)_2O_3$ as a function of Mo doping at 10 K (black symbols, triangles: I-type phase, circles: M-type phase) and 300 K (open circles, from Ref. [8]).

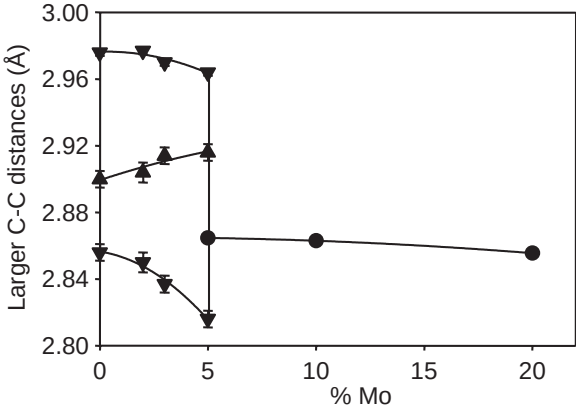

Fig. 10. Nearest cation–cation distances in the π_h plane as a function of Mo doping at 10 K. Triangles = I-type phase, circles = M-type phase.

thermal X-ray diffraction patterns between 10 K and RT, the expected refinement accuracy is lower, but we nevertheless carried it out.

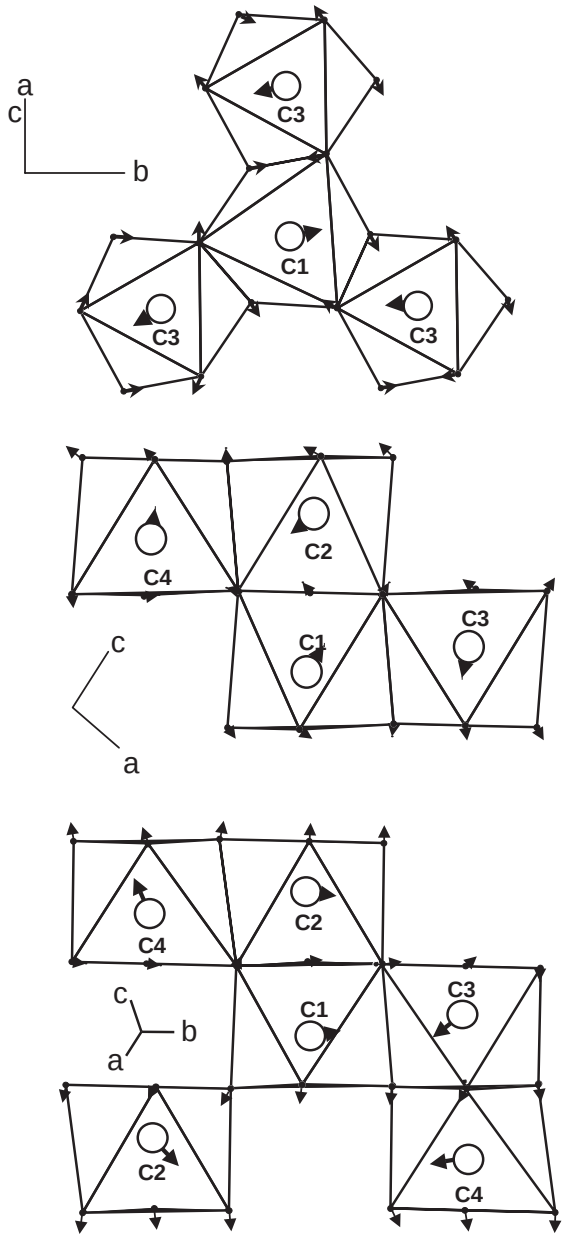

Fig. 11. Atomic shifts (exaggerated) in the I-type phase at 10 K upon Mo doping (from top to bottom: in the π_h, π_1 and π_2 planes, respectively). Same cationic numbering as in Fig. 7.

The main results in terms of most significant interatomic distances are displayed in Figs. 14 and 15. They compare the thermal evolution of mean cation–anion and cation–cation distances in both I- and M-type phases. Within the error bars, they seem to vary in a somewhat different manner. Whereas in the rhombohedral high-temperature phase, all interatomic distances (except perhaps the C–O distance of undoped V_2O_3) increase with temperature, this is not the case in the monoclinic low-temperature phase, where the same distances either decrease or remain constant upon heating. This behavior is consistent with the global

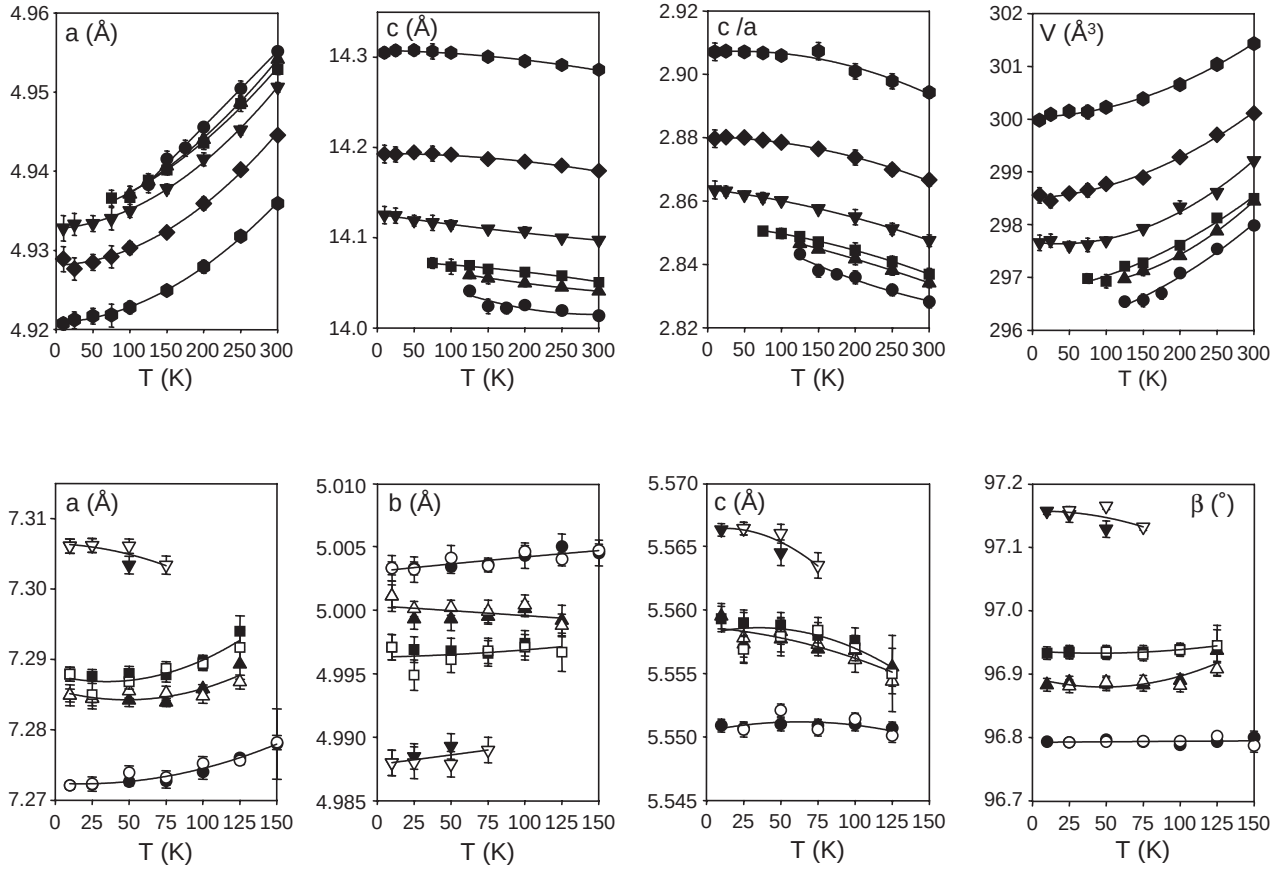

Fig. 12. Thermal evolution of cell parameters for different Mo-doping rates in $(V_{1-x}Mo_x)_2O_3$. Upper row: a, c, c/a, and cell volume for the M-type phase. Lower row: a, b, c, and β for the I-type phase. Symbols: • = 0% Mo, ▲ = 2% Mo, ■ = 3% Mo, ▼ = 5% Mo, ◆ = 10% Mo, ⬢ = 20% Mo while cooling (identical open symbols upon heating the I-type phase).

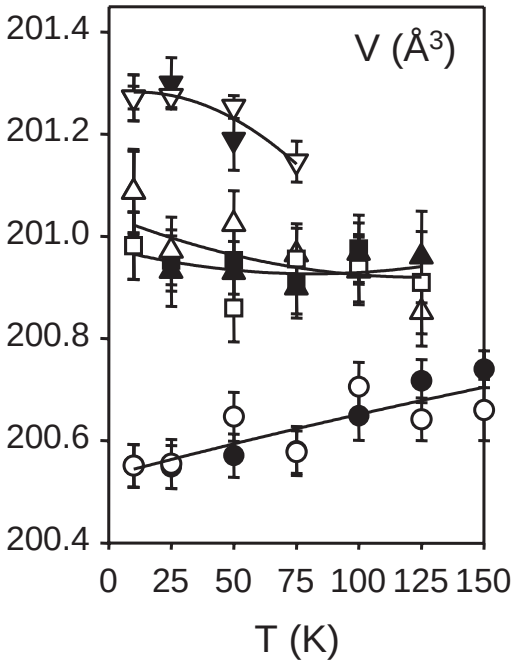

Fig. 13. Thermal evolution of cell volume for different Mo-doping rates in the I-type phase of $(V_{1-x}Mo_x)_2O_3$ showing the negative thermal expansion coefficient of the doped phases. Same symbols as Fig. 12.

thermal expansion of the M-type phase, and the negative expansion coefficient of the I-type phase of doped sesquioxides.

The narrower thermal and compositional ranges, together with (and in a sense inducing) smaller atomic displacements within the I-type phase, prevent us from having a clearer image of the thermal evolution of the monoclinic structure. The thermal behavior of the M-type structure appears to be somewhat easy to depict. The effect of cooling on the anionic movements depends on the level of Mo doping. For undoped V_2O_3, the oxygen x parameter increases and the cationic octahedral coordination tends to become more regular when temperature is lowered to the transition temperature. The effect is of the same type, but with a smaller amplitude for the 2% doped compound, whereas the oxygen positions practically do not change with temperature for 3% and 5% doped sesquioxides. Finally, the opposite tendency is noted for 10% and 20% Mo-doped oxides, where oxygen abscissa decreases and coordination octahedra distort slightly upon cooling. The main evolutions described above are depicted in Fig. 16. The octahedral regularization (or distortion) follows roughly the same mode as that induced by Mo

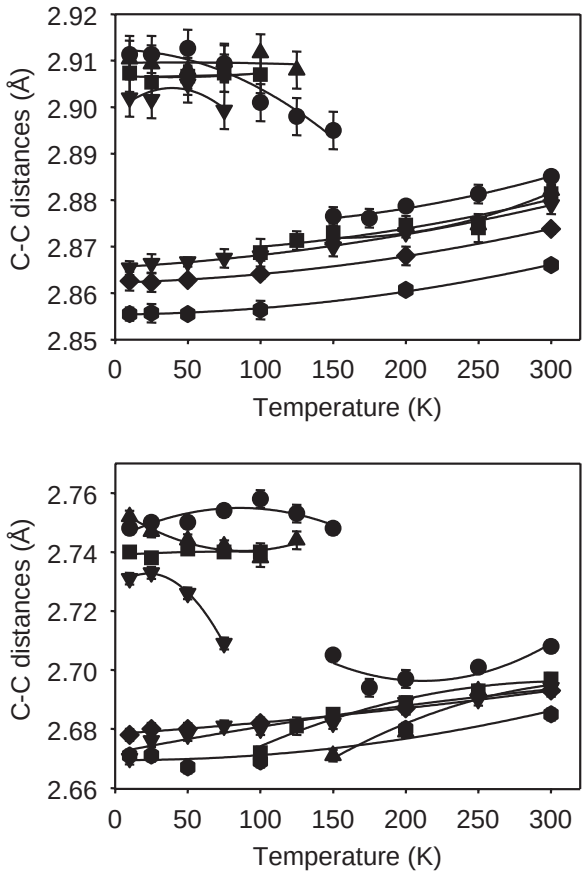

Fig. 14. Thermal evolution of average interatomic C–C distances in edge-sharing (top) and corner-sharing (bottom) octahedra of $(V_{1-x}Mo_x)_2O_3$ for different doping rates. Same symbols as Fig. 12.

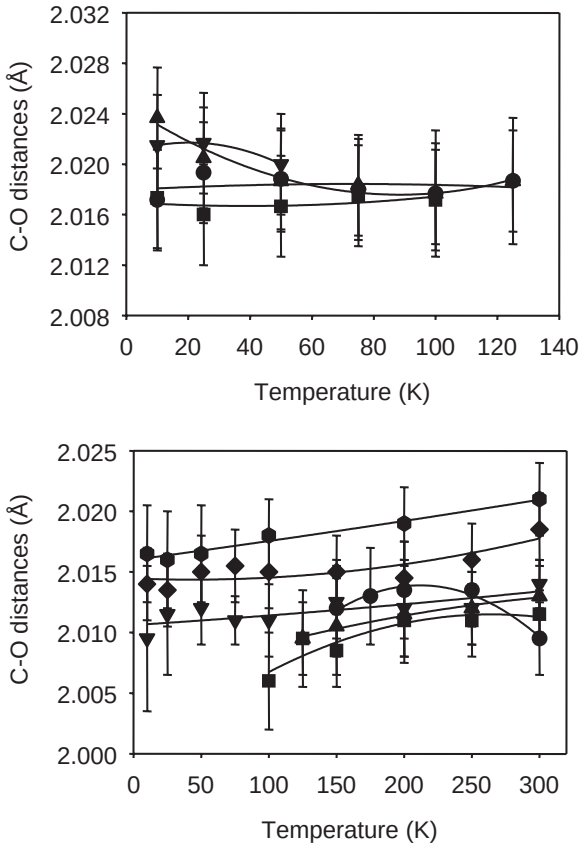

Fig. 15. Thermal evolution of average interatomic C–O distances in the I-type (top) and M-type (bottom) phases of $(V_{1-x}Mo_x)_2O_3$ for different doping rates. Same symbols as Fig. 12.

doping at constant T (see [8, Section 3.2]): enlargement of common faces of bioctahedral units and expansion of opposite ones (or reverse).

5. Summary and conclusion

In this study we have undertaken the low-temperature crystal structure study, between 10 K and room temperature, of Mo-doped vanadium sesquioxides, both as a function of Mo content and temperature. At first sight, one would expect a somewhat similar effect of Mo doping and of temperature, since Mo^{3+} is larger than V^{3+} and induces bond lengthening with oxide ligands, as in the usual thermal expansion. However, competing effects such as the formation of Mo–Mo metal bonding [8] complicates the comparison. As a matter of fact, at 10 K the effect of Mo doping on the main interatomic distances is comparable to that observed at room temperature: an increase of cation–oxygen distances, and decrease of cation–cation distances, whatever the structural type (monoclinic or rhombohedral). The transition from one structural type to the other is accompanied by an abrupt decrease of all distances in the more conducting phase. The same effect is observed when the transition is driven thermally. Within each phase type however, the thermal evolution appears to be different in each structure type, and from that of Mo doping. In the M-type phase, all interatomic cation–oxygen and cation–cation distances increase with temperature, whereas in the I-type phase, they both have a tendency to either decrease or remain constant. This unusual behavior is due to the negative thermal

Table 3
Comparison of the effects of Mo doping and temperature on the increase (+) or decrease (−) of some crystallographic parameters of the M- and I-type phases of $(V_{1-x}Mo_x)_2O_3$

	Mo-doping (M-phase)	Mo-doping (I-phase)	Temperature (M-phase)	Temperature (I-phase)
c/a	+	+	−	−/=
Cell volume	+	+	+	−/=
C–O distances	+	+	+	−/=
C–C distances	−	−	+	−/=

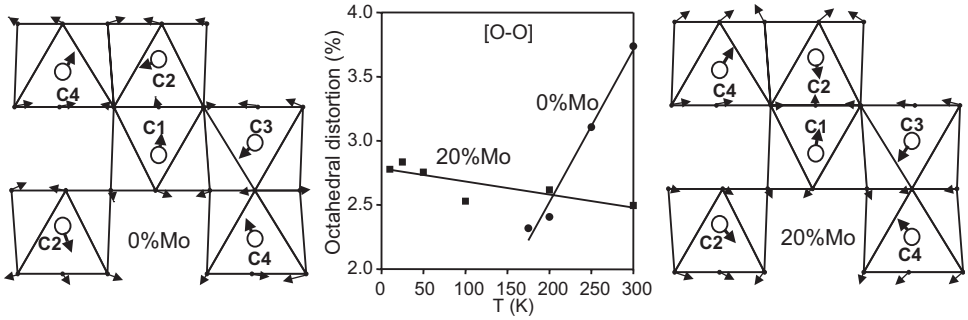

Fig. 16. Thermal evolution of octahedral distortion (center, relative overall deviation from the average nearest [O–O] distances) and atomic shifts (exaggerated) in the M-type phases of V_2O_3 (0% Mo) and $(V_{0.8}Mo_{0.2})_2O_3$ (20% Mo). Same cationic numbering as in Figs. 7 and 11.

expansion coefficient of Mo-doped monoclinic phases. A qualitative summary of these results is presented in Table 3.

Since thermal crystallographic studies of the vanadium sesquioxide system are not very common, it is expected that the present study provides a useful contribution to a better knowledge of some of its properties.

Acknowledgments

The authors thank Dr. A. Desert and M. G. Ripault for their kind help and technical assistance with low-temperature X-ray diffraction.

References

[1] M. Foex, C. R. Acad. Sci. 223 (1946) 1126.
[2] M. Foex, C. R. Acad. Sci. 229 (1949) 880.
[3] N.F. Mott, Proc. Phys. Soc. A 62 (1949) 416.
[4] J.M. Honig, J. Solid State Chem. 45 (1982) 1.
[5] M. Yethiraj, J. Solid State Chem. 88 (1990) 53.
[6] P. Lacorre, C. Tenailleau, Solid State Sci. 4 (2002) 217.
[7] C. Tenailleau, Ph.D. Thesis, University of Le Mans, France, 2001.
[8] C. Tenailleau, E. Suard, J. Rodriguez-Carvajal, M.-P. Crosnier-Lopez, P. Lacorre, Chem. Mater. 14 (2002) 3569.
[9] J. Rodriguez-Carvajal, Physica (Amsterdam) 192B (1993) 55.
[10] P. Dernier, M. Marezio, Phys. Rev. B 2 (1970) 3771.
[11] J.S.O. Evans, T.A. Mary, A.W. Sleight, J. Solid State Chem. 133 (1997) 580.
[12] W. Bao, C. Broholm, S.A. Carter, T.F. Rosenbaum, G. Aeppli, S.F. Trevino, P. Metcalf, J.M. Honig, J. Spalek, Phys. Rev. Lett. 71 (1993) 766.